sciendo

Int. J. of Applied Mechanics and Engineering, 2022, vol.27, No.3, pp.163-170
DOI: 10.2478/ijame-2022-0042

INFLUENCE OF MULTI EXTRUSION DIE PROCESS ON MECHANICAL AND CHEMICAL BEHAVIOR OF 2024-T3 ALLOY

Ahmed Ibrahim RAZOOQI
Technical Engineering College - Baghdad, Middle Technical University, Baghdad, IRAQ

Naseer M. ABBAS* and Sara Saad GHAZI
Institute of Technology - Baghdad, Middle Technical University, Baghdad, IRAQ.
E-mail: naseerma2@gmail.com; nabbas@mtu.edu.iq

In this paper, a cold multi-pass extrusion process for a *15mm* in diameter solid 2024-T3 aluminum alloy rod was carried out using three dies to obtain three different diameters of *14mm, 13mm*, and *12mm*. The microstructure, hardness, and corrosion behavior were investigated before and after the extrusion process. Load-Displacement data were recorded during each extrusion process. The electrochemical corrosion test was made in a *3.5 wt.*% NaCl solution using potentiostat instrument under static potentials test. Corrosion current was recorded to determine the corrosion rate for specimens. The results showed that the extrusion load increased with the number of extrusion passes, which is also seen in hardness test results. In addition, the corrosion rate decreased with the increase in the number of extrusion passes. This is due to severe plastic deformation, which generates a fine grain structure of (AlCu) and (AlCuMg) components.

Keywords: Al 2024-T3, extrusion, plastic deformation, electrochemical corrosion.

1. Introduction

Aluminum (2024-T3) is a widely used alloy in a variety of engineering applications for its high strength, e.g. in aircraft structures. The applications of this alloy require specific properties, like high strength and hardness, high toughness, fatigue crack growth resistance, as well as high corrosion resistance. Researchers have been studying and improving the mechanical and chemical properties of Al 2024 for specific applications through different mechanical and chemical processes, like forming processes, chemical and heat treatments, and metal powders additives. (Abdollahi *et al*. [1]; Ashwath *et al*. [2]; Guia-Tello *et al*. [3]; Fang *et al*. [4]). Extrusion is a widely used engineering process in the construction, aerospace, energy, and automotive industries. It is one of the most frequently used metal forming techniques, and has a growing significance in industry. Extrusion is a forming process a metal to a wanted form by pushing it through a die cavity using hydraulic pressure [5, 6]. Cold extrusion is done at or near room temperature compared to hot extrusion, which has many advantages such as the absence of oxidation, greater material strength, good surface finish, and low cost. Aluminum, lead, tin, copper, and other low melting temperature materials are often used in cold extrusion. Collapsible tubes, shock absorber cylinders, fire extinguisher cases and gear blanks are all well-known cold extrusion products. On the other hand, cold extrusion requires high pressure and can result in product defects.

Extrusion processing has the benefit of allowing varied microstructures to be created by adjusting process parameters, resulting in superior mechanical and chemical characteristics through the optimization of processing conditions. Many researchers have investigated various extrusion parameters for both cold and hot processes. A prediction of grain size and precipitation is of increasing importance in order to design the process by adjustment of parameters such as punch speed, temperatures and quenching [7, 8]. Metal corrosion is an electrochemical process that causes material characteristics to deteriorate due to an unavoidable reaction with

* To whom correspondence should be addressed

the environment. Corrosion is most commonly associated with metallic materials, but it can harm any type of material; for example, selective dissolution can cause ceramics to deteriorate [9, 10].

The purpose of the current study is to investigate the influence of multiple cold extrusion passes on microstructures, hardness and corrosion behavior for AA2024–T3 aluminum alloy.

2. Experimental work

2.1. Material used

The material used in this study is 2024-T3 Aluminum alloy rod of *15mm* in diameter. The chemical analysis was carried out using the ARL spectrometer system and the findings are provided in Tab.1. The mechanical properties of 2024 Al alloy are illustrated in Tab.2.

Table 1. Chemical composition of 2024-T3 Al alloy.

Element wt. %	Al	Ti	Cr	Zn	Si	Fe	Mn	Mg	Cu
Real value	*92.5*	*0*	*0.06*	*0.11*	*0.41*	*0.3*	*0.55*	*1.5*	*4.5*
Standard value [11]	*Rem.*	*0 -0.15*	*0 -0.1*	*0 -0.25*	*0 -0.5*	*0 -0.5*	*0.3 -0.9*	*1. 2-1.8*	*3.8 -4.9*

Table 2. Mechanical properties of 2024 -T3 Al alloy [11].

Property	Density $\left(Kg/m^3\right)$	Ult. Tensile Strength (MPa)	Yield Strength (MPa)	Young's Modulus (GPa)	Elongation $(\%)$	Hardness (HRB)
Value	*2780*	*480*	*360*	*73*	*10*	*38*

2.2. Classification of specimens

The classification of the specimen utilized in this study is provided in Tab.3. This classification will be used throughout the rest of this paper.

Table 3. Classification of specimens.

Specimen's symbol	State of Specimen
A	As received
B	Extrusion to *14mm*
C	Extrusion to *13mm*
D	Extrusion to *12mm*

2.3. Extrusion process

The 2024–T3 Al alloy rods were extruded, using three different tool steel dies with different inner diameters of *14*, *13*, and *12 mm*, respectively, on an Instron machine. After each extrusion process, load-displacement data, hardness, and microstructure for extruded rods were recorded for later comparison and study.

2.4. Load-displacement data

During the extrusion process for each pass, the Load-displacement data were recorded. Figure 1 shows the Load-displacement curves for specimens B, C, and D.

2.5. Residual stress measurement

The strain from the base metal and extrusion process specimens, as well as the crystal lattice, are measured with a computerized (Lab XRD-6000 Shiatsu X-RAY Diffract meter), and the strain is used in the brag law to calculate the compressive residual stress obtained from the device. The results are shown in Tab.4.

2.6. Surface roughness

The average roughness (Ra) and peak roughness (Rt) of corrosion samples were measured at the exterior face zone. A test machine (pocket surface) is used for this purpose. The results are shown in Tab.5.

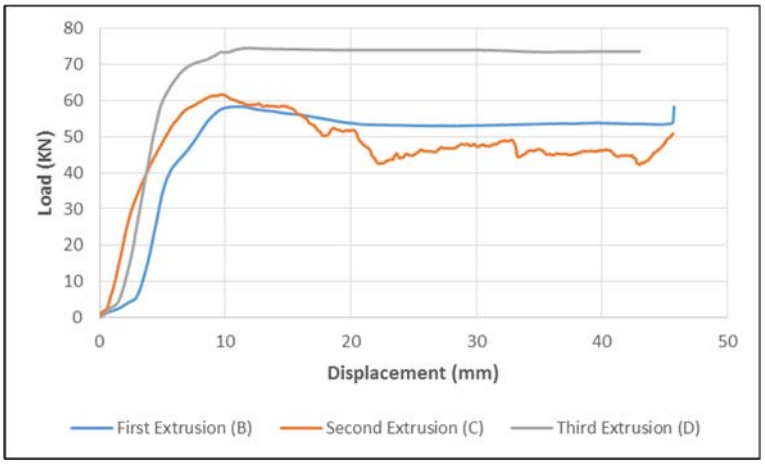

Fig.1. Relationship between load-displacement.

Table 4. Residual stress result for all specimens.

Specimens symbol	A	B	C	D
Residual Stress value	*-17.5*	*-110*	*-140*	*-160*

Table 5. Surface roughness results.

Specimens symbol	A	B	C	D
Average surface roughness (µm)	*0.19*	*0.3*	*0.23*	*0.08*

3. Results

3.1. Microstructure test

The base and extruded sample microstructures were created in a series of processes. Using SiC emery paper of various grits, wet grinding with water was performed (*240*, *320*, *500*, *800*, and *1000*). The samples were polished by using diamond paste of size (*1µm*) with a special polishing cloth. They were cleaned with water and alcohol and dried with hot air. The samples were etched with an etching solution (Keller's reagent) consisting of *95ml* distill water, *2.5ml* HNO3, *1.5ml* HCl and *1ml* HF. They were washed

after that with water and alcohol and dried in an oven. The samples were examined by Nikon ME-600 optical microscope provided with a NIKON camera, DXM-1200F.

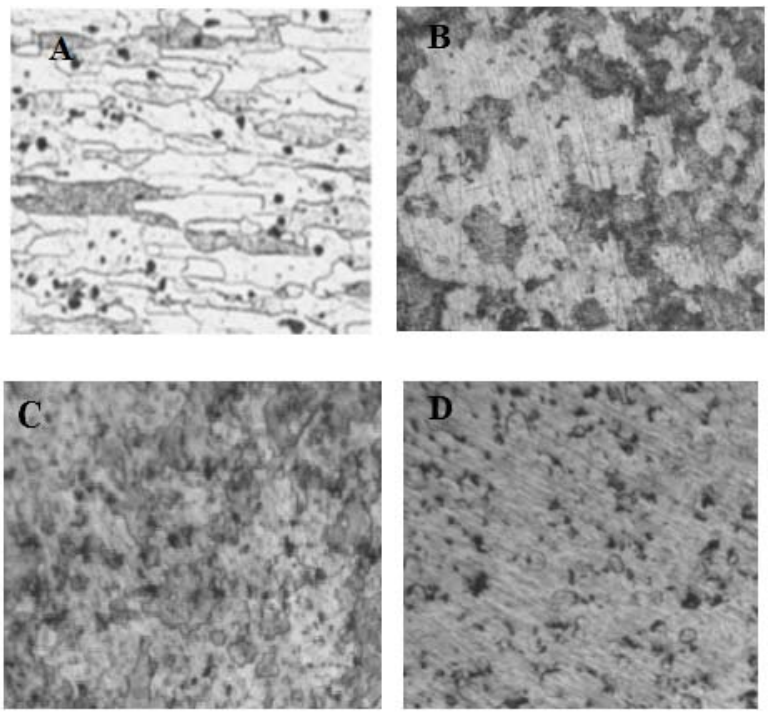

Fig.2. Microstructure for specimens A, B, C, and D at 100x.

3.2. X-ray diffraction test

The x-ray diffraction inspection was performed on the produced samples, which included 2θ scanning from (*20* to *80*) at (*0.020*) pace size for (*0.2000deg*) each step using a (CuK) radiation source (*1.541A*) with a current of *30mA* and a voltage of (*40kV*).

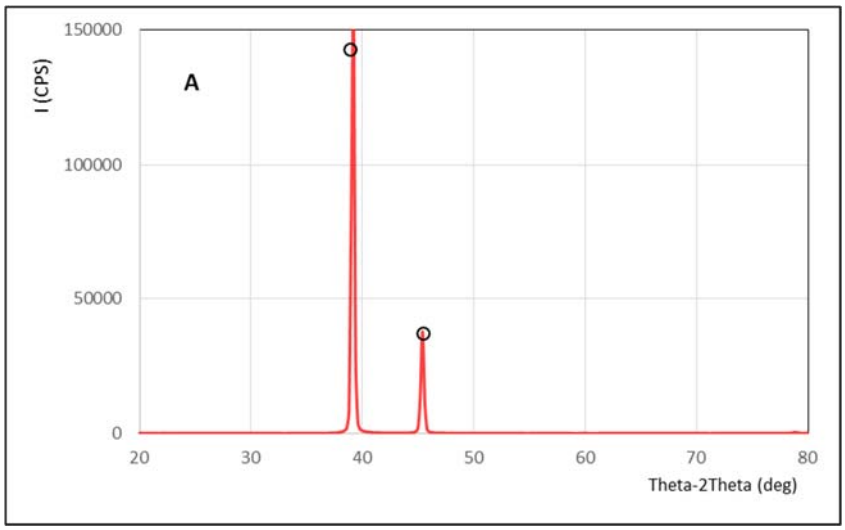

Fig.3a. The X-ray diffraction patterns for tests specimen A represents phases.

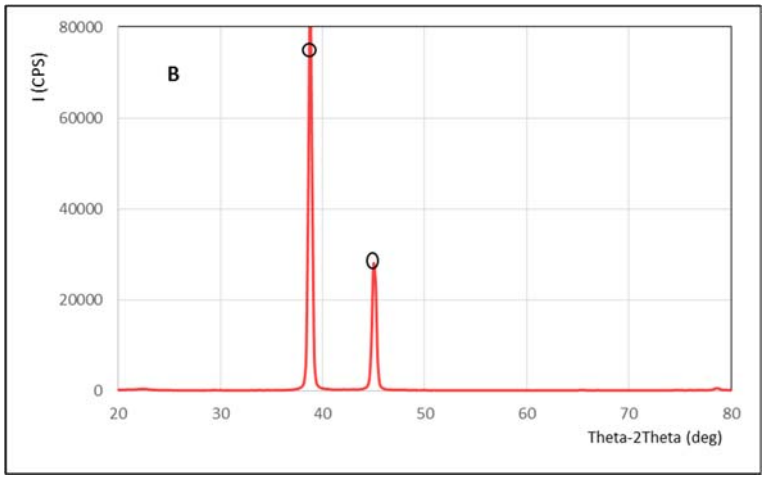

Fig.3b. The X-ray diffraction patterns for tests specimen B represents phases.

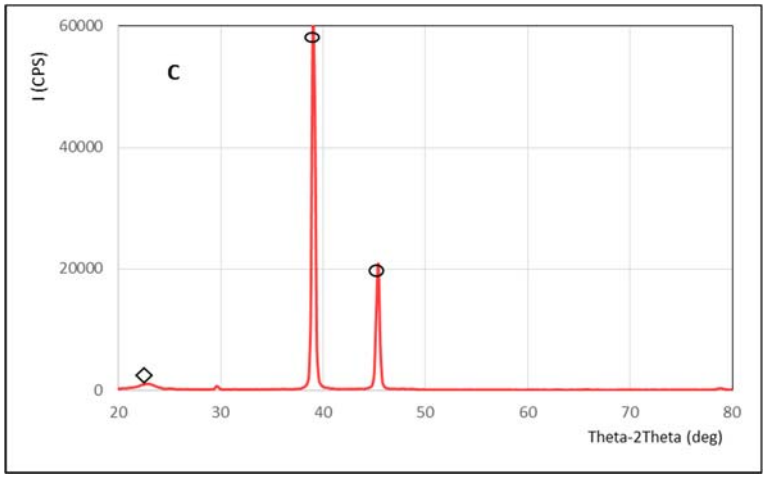

Fig.3c. The X-ray diffraction patterns for tests specimen C represents phases.

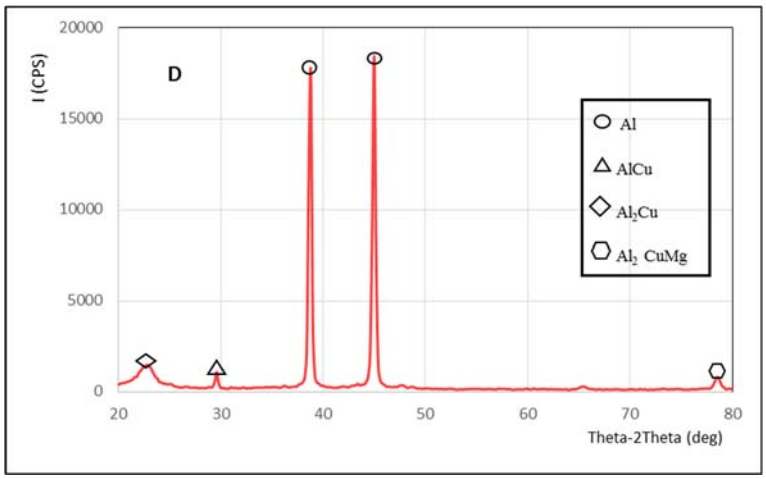

Fig.3d. The X-ray diffraction patterns for tests specimen D represents phases.

As indicated in Fig.3, phase identification was investigated by computing the d-spacing (interlayer spacing and Bragg angle in degrees) for four groups of extruded specimens using Bragg's law (1). It was discovered that as the number of extrusions increases, the number of precipitation phases such as Al, AlCu, Al2Cu, and AL2CuMg increases. Because of the increase in hardness, these phases contributed to decreases in corrosion rate.

3.3. Hardness test

Hardness test results for all specimens are listed in Tab.6. The test was carried out using a Rockwell B Scale Hardness Testing Device with a ball diameter of *1.59mm* and a load of *100kg*. The test was repeated three times for each specimen, and the average value is shown in Tab.6.

Table 6. Hardness test results.

Specimen Symbol	A	B	C	D
Hardeners value Kg/mm^2	*37.6*	*47*	*60*	*72*

3.4. Corrosion test

After each extrusion process, the extruded specimens, as well as the base metal, were subjected to a corrosion test. Based on the ASTM standard, (G70-30) the specimens dimension were prepared .The test was performed for specimens in seawater, which was prepared from a solution of *3.5%* NaCl in distilled water at *6.6 PH*. Corrosion potential (Ecorr) and corrosion current (Icorr) are two of the most important corrosion parameters. The sweep ranged from *-250* to *+250mV* in relation to open cycle polarization (OCP). The scan rate is fast (10) *mV/sec* and describes the velocity of the potential sweep in *mV/sec*. the tests were made using a potentiostate multi-channel WENKING Mlab and a corrosion-measuring device (SCI-Mlab) from Bank Electronics-Intelligent Control GmbH, Germany. As indicated in Eq.(3.1) (Oladele *et al*. [12]), the rate of corrosion agreed with the Tafel equation below.

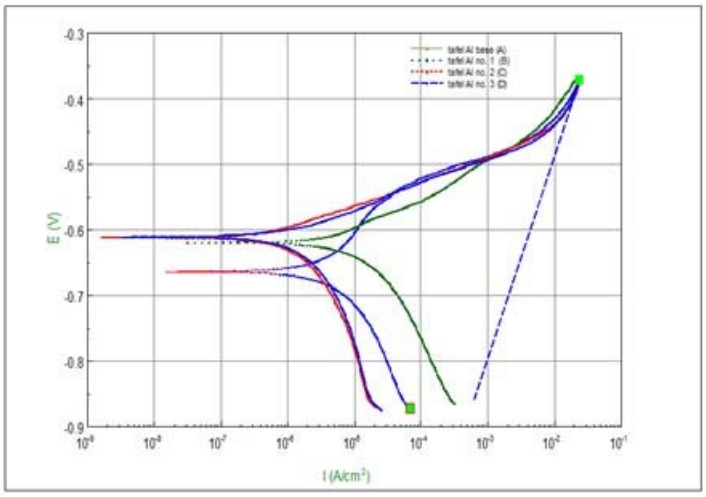

Fig.4. Electrochemical behavior polarization for all specimens.

Corrosion test results are presented in Tab.7 and Fig.4.

$$C.R = 0.13 * Icorr * E * W / \rho \tag{3.1}$$

where:

C.R: corrosion rate in *mpy* (mils per year).
Icorr : corrosion current in (*mA*).
E.W: equivalent weight of the corroding species.
ρ: density of the corroding species (g/cm^3).

Table 7. Corrosion test results for specimens A, B, C, and D.

Specimens Sample	I corr[$\mu A/cm^2$]	E_{corr}.(Volts)	Corrosion Rate (*mpy*)
A	*9.0084E-06*	*-0.62029*	*0.098131*
B	*5.9042E-06*	*-0.66413*	*0.069264*
C	*1.0047E-06*	*-0.61205*	*0.010944*
D	*1.4597E-06*	*-0.61143*	*0.017124*

4. Discussion

The microstructural evolution, hardness, and corrosion behavior of 2024-T3 Al alloy rod subjected to a multi-pass extrusion process were investigated. Figure 2 depicted the microstructure of AA 2024-T3. Specimen (A) contains elongated grains which gives the alloy a good corrosion resistance. In addition, the uniform precipitates of a very fine (ALCu), where the main alloying element is copper (Cu) are shown in Tab.1. It provides a significant increase in strength by allowing precipitation hardening. Due to severe plastic deformation of the material, a fine grain structure is seen after the extrusion process for specimens B, C, and D. The microstructure becomes finer as the number of extrusion passes increases. Evolution in microstructure was also characterized by the X-ray diffraction test (XRD), where the main phases formed were (AlCu, Al2Cu, and Al2CuMg). Due to dedimentation and grain size refinement, as well as strain hardening of the specimens, which happened because of multiple extrusion passes, a significant impact on hardness is noticed in specimens B, C, and D. This is also obvious from load-displacement curves in Fig.1, where the load required for extruding the material increased in the third pass. The above findings are consistent with what was found in Guia-Tello *et al*. [3]; Anghelina *et al*., [13]; [14].

The corrosion behavior and corrosion rate of Al-alloys mainly depend on the heterogeneity of their microstructure. The microstructure electrochemical behavior is directly proportional to the number of present phases, as discussed earlier in the XRD test. Figure 5 shows the polarization curves for specimens A, B, C, and D. These curves represent the cathodic and anodic areas, which determine the corrosion potentials and corrosion current. The corrosion rate is very high in the base metal alloy (specimen A) due to the presence of chloride ions (Talbot and Talbot [15]; Trethewey and Chamberlain [16]). After implementing multiple extrusion passes, the corrosion rate was improved for specimens B, C, and D due to significant alterations in the microstructure. The corrosion behavior for the base alloy (A) differs substantially after the extrusion process, where it has a high corrosion current (Icorr), or a low corrosion resistance. This is because of the microstructure uniformity that occurs after the extrusion process. The formed precipitates facilitate matrix anodic dissolution. In addition, extruded specimens have a higher negative corrosion potential (Ecorr) than the base alloy. When comparing the results of the electrochemical corrosion test with the results after extrusion, the extrusion process for one pass produced a high corrosion rate compared with corrosion in specimen (B).

5. Conclusions

1. Due to severe plastic deformation and material flow, a grain refinement zone was produced due to multiple extrusion processes.
2. The hardness of the extruded product is mostly determined by the distribution of precipitates rather than the grain size.
3. Corrosion resistance for the extruded rod was found to be better than that for the base alloy.

Acknowledgment

The authors would like to thank Dr. Mustafa K. Ismael, and Ms. Khaira S. Hassan / Institute of Technology - Baghdad, Middle Technical University**,** Baghdad, IRAQ for their help and support.

Nomenclature

$C.R$ – corrosion rate in *mpy* (mils per year).
$Icorr$ – corrosion current in (mA).
$E.W$ – equivalent weight of the corroding species.
ρ – density of the corroding species (g/cm^3).

References

[1] Abdollahi A., Alizadeh A. and Baharvandi H. (2014): *Dry sliding tribological behavior and mechanical properties of Al2024–5 wt.%B4C nanocomposite produced by mechanical milling and hot extrusion*.– Materials and Design, vol.55, pp.471-481.

[2] Ashwath P., Joel J., Kumar H. G., Xavior M., Goel A., Nigam T. and Rathi M. (2018): *Processing and characterization of extruded 2024 series of aluminum alloy*.– Materials Today: Proceedings, vol.5, pp.12479-12483.

[3] Guia-Tello J.C., Garay-Reyes C.G., Medrano-Prieto H.M., Esparza-Rodriguez M.A., Maldonado-Orozco M.C., Rodriguez-Cabriales G. and Martinez-Sanchez R. (2019): *Effect of the age-hardening time on the microstructure of cold rolled Al2024 alloy*.– Microsc. Microanal., vol.25, No.2, pp.2626-2627.

[4] Fang G., Ma L. and Zeng P. (2008): *Hot formability investigation of the pre-extruded 2024 aluminum alloy*.– The 9th International Conference on Technology of Plasticity, pp.328-332.

[5] Crispim V.R. and Silva J.J.G. (1998): *Detection of corrosion in aircraft aluminum alloys*.– Applied Radiation and Isotopes, vol.49, No.7, pp.779-782.

[6] Khan I., Ismail U., Noman D., Siddiqui M. and Shahzad M. (2017): *Effect of process parameters on formability of aluminum 2024*.– Journal of Space Technology, vol.7, No.1, pp.7-11.

[7] Hinesley C.P. and Conrad H. (1973): *Effects of temperature and ram speed on the flow pattern in axisymmetric extrusions of 2024 Al alloy*.– Materials Science and Engineering, vol.12, pp.7-58.

[8] Hu L., Li Z. and Wang E. (1999): *Influence of extrusion ratio and temperature on microstructure and mechanical properties of 2024 aluminum alloy consolidated from nanocrystalline alloy powders via hot hydrostatic extrusion*.– Powder Metallurgy, vol.42, No.2, pp.153-156.

[9] Lou G., Xu S., Teng X., Ye Z., Jia P., Wu H., Leng J. and Zuo M. (2019): *Effects of extrusion on mechanical and corrosion resistance properties of biomedical Mg-Zn-Nd-xCa alloys*.– Materials, vol.12, No.1049, pp.1-13.

[10] Shaw B.A. and Kelly R.G. (2006): *What is corrosion?*.– The Electrochemical Society Interface, pp.24-26.

[11] William H. (1985): *Properties and Selection: Non Ferrous Alloys and Pure Materials*.– Metal Handbook, vol.9.

[12] Oladele I.O., Betiku O.T., Okoro A.M., Eghonghon O. and Saliu L.O. (2018): *Comparative investigation of the mechanical properties and corrosion behavior of dissimilar metal weld fusion zone, heat affected zones and base metals*.– Annals of Faculty Engineering Hunedoara, International Journal of Engineering, pp.187-191.

[13] Anghelina F., Ionita I., Ungureanu D., Stoian E., Popescu I., Bratu V., Petre I., Popa C. and Negrea A. (2017): *Structural aspects revealed by X-Ray Diffraction for aluminum alloys 2024 type*.– Key Eng. Materials, vol.750, pp.20-25.

[14] Metals Handbook, (1990): *Properties and Selection: Nonferrous Alloys and Special-Purpose Materials*.– vol.2, ASM International 10th Ed.

[15] Talbot D.E., and Talbot J.D. (1998): *Corrosion Science and Technology*.– CRC Press LLC.

[16] Trethewey R.K. and Chamberlain J. (1996): *Corrosion for Science and Engineering*. – 2nd Edition, Longman Group Limited.

Received: April 4, 2022
Revised: June 3, 2022